A transparent metamaterial to manipulate electromagnetic wave polarizations

Wujiong Sun, Qiong He, Jiaming Hao, and Lei Zhou*

State Key Laboratory of Surface Physics and Key Laboratory of Micro and Nano Photonic Structures (Ministry of Education), Fudan University, Shanghai 200433, China

**Corresponding author: phzhou@fudan.edu.cn*

Received November 16, 2010; revised February 14, 2011; accepted February 15, 2011; posted February 15, 2011 (Doc. ID 138185); published March 10, 2011

We design an anisotropic ultrathin metamaterial to allow *perfect* transmissions of electromagnetic (EM) waves for two incident polarizations within a common frequency interval. The transparencies are governed by different mechanisms, resulting in significant differences in transmission phase changes for two polarizations. The system can thus manipulate EM wave polarizations efficiently in transmission geometry, including polarization conversion and rotation. Microwave experiments performed on realistic samples are in excellent agreement with numerical simulations.

OCIS codes: 160.3918, 240.6680, 160.1190.

It is highly desirable to efficiently control the polarization of electromagnetic (EM) waves [1], due to many application requests [2]. Conventional methods to manipulate the polarization of light (based on Faraday, Kerr, birefringence effects, etc.) typically require a system much thicker than wavelength, which is inconvenient for low-frequency applications [3]. Although an optical grating can be very thin, it suffers the energy loss problem, since the system is not perfectly transparent [1,3].

Metamaterials, artificial materials composed by resonant microstructures to exhibit arbitrary values of effective ε and μ [4–6], open a new way to manipulate polarization. It was recently shown that a specifically designed metamaterial reflector can efficiently manipulate EM wave polarizations [7]. The device is much thinner than wavelength and does not suffer the energy loss issue, since it perfectly reflects EM waves [7]. However, the reflection geometry makes it inconvenient for practical applications due to the interference between incident and reflected waves. Subsequently, several other metamaterial systems were proposed to manipulate polarization in transmission geometry [8–12]. While these proposals [8–12] can avoid the interference problem, the devices are typically *not* perfectly transparent for EM waves, so the energy loss issues remain unsolved.

Here we design an anisotropic metamaterial to manipulate EM wave polarizations in transmission geometry. The proposed device is much thinner than wavelength, is *perfectly transparent* for EM waves at the working frequency, and can manipulate the EM wave polarizations efficiently. Microwave experiments are performed on realistic samples to demonstrate the polarization manipulation effects, with obtained results agreeing well with numerical simulations.

Our system is a laterally *anisotropic* ABA structure consisting of three metamaterial layers, each two separated by a distance d. As schematically shown in Fig. 1(a), layer A is an electric metamaterial with periodically arranged resonant microstructures, while layer B is a metallic mesh. This design is motivated by a previous study in which a series of *perfect* transmission peaks were found in a laterally *isotropic* ABA system [13]. If we utilize the lateral *anisotropy* to purposely make the system *transparent* for both incident polarizations at a common frequency but with *different* transparency mechanisms, then the transmission coefficients of the system must be $t_x = e^{i\varphi_x}$, $t_y = e^{i\varphi_y}$, where $\varphi_x \neq \varphi_y$. When $\Delta\varphi = \varphi_y - \varphi_x$ is large, the polarization manipulation can be easily realized.

We first employed the finite-element method (FEM) [14] to numerically study the transmission properties of the system for $\vec{E}\|\hat{x}$. Assuming $d = 3$ mm, we calculated the normal-incidence transmission spectrum and plotted the results in Fig. 2(a) as open circles. Three *perfect* transmission peaks are observed at 2.1, 2.8, and 6.6 GHz. To understand the nature of these peaks, we varied the interlayer distance d to recalculate these peak frequencies and plotted the results in Fig. 2(b) as symbols. As d increases, the first two peaks approach each other and merge together as d exceeds a critical value. Meanwhile, the third peak approaches a limiting frequency ~7.1 GHz as d increases.

Figure 2(b) implies that the three peaks might have different physical origins. The first two peaks are easily identified as those discussed in [13], which can be explained by the effective medium theory (EMT). By comparing FEM calculations on realistic structures and transfer-matrix method (TMM) calculations on homogeneous slabs [13], we found that individual A and B layers can be modeled by two homogeneous slabs with

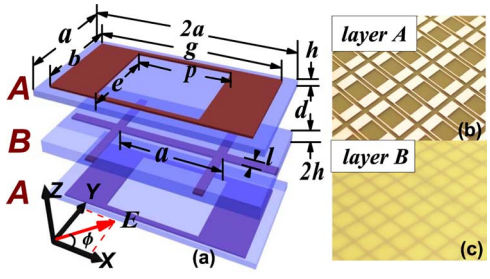

Fig. 1. (Color online) (a) Unit cell structure of our design: $a = 12$, $b = 10$, $g = 21.3$, $e = 9$, $p = 11$, $l = 1$, and $h = 0.6$ mm, and the metal thickness is 0.018 mm. All substrates have $\varepsilon = 3.5$, and for layer B the metallic mesh is sandwiched between two identical substrates. Pictures of fabricated (b) A and (c) B layers.

$\varepsilon_A^x = 20.2 + 1917/(5.47^2 - f^2)$ and $\varepsilon_B = 4.483 - 623.1/f^2$, where f denotes the frequency measured in gigahertz. Replacing the realistic layers A and B by two homogeneous slabs with the above permittivity, we employed the TMM to calculate the transmission spectrum for the system with $d = 3$ mm and plotted the results in Fig. 2(a) as a solid line. The TMM results reproduced the first two peaks in the FEM spectrum, but the third peak at ~6.6 GHz is missing. We next employed the TMM to calculate the transmission peaks in different d cases and plotted the results as solid lines in Fig. 2(b). Again, the TMM calculations reproduced the general behaviors of the first two peaks [13]. However, the third peak does not exist in TMM.

We found that the third peak is governed by the extraordinary optical transmission (EOT) mechanism [15–17]. Because ε_B is negative, p-polarized surface plasmon polaritons (SPPs) exist on the surface of layer B. Generally, such modes cannot be excited by propagating waves due to the wave-vector mismatch. However, when a layer A is placed near the layer B, the periodicity of layer A provides a reciprocal vector to compensate the wave-vector mismatch so that the SPP modes can be "seen" by incident plane waves, leading to the EOT phenomenon. Numerical simulations confirmed this conjecture. Depicted in Fig. 3(a) are the field distributions inside an ABA structure at the transparent frequency. Only E_x, E_z, and B_y exist here, which distribute periodically on both surfaces of layer B with periodicity *identical* to that of layer A. These are clear features of a p-polarized SPP mode modulated by Bragg scatterings. We further calculated the dispersion of SPPs on layer B with the obtained ε_B and drew the dispersion curve in Fig. 3(b) as a solid line [18,19]. Clearly, the SPP dispersion lies below the light line (dashed line) and thus cannot be excited by a normal-incident plane wave. However, with an additional reciprocal vector provided by layer A ($G = 2\pi/(2a)$), an SPP mode can be excited, leading to the EOT at 7.1 GHz, which matches perfectly with the limiting frequency observed in Fig. 2(b). The deviations from the limiting value in the small d case [see Fig. 2(b)] are caused by the strong disturbances in the SPP dispersion contributed by layer A. We note that the transmittance at the EOT is ~100% based on full-wave FEM

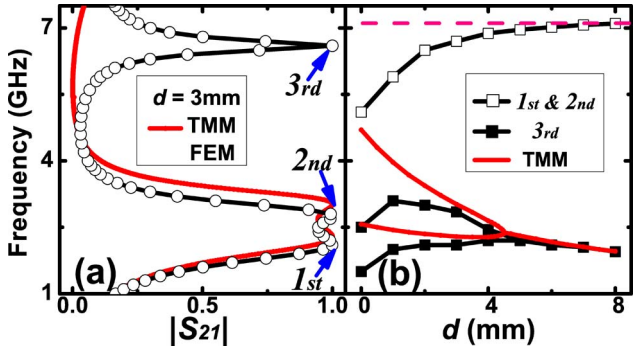

Fig. 2. (Color online) (a) Transmission spectra (S_{21}) for the ABA structure with $d = 3$ mm, calculated by FEM and TMM. (b) Transmission peak frequencies as functions of d, calculated by FEM and TMM. The thicknesses of the homogenized A and B layers are assumed to be 0.6 and 1.2 mm, respectively, in TMM.

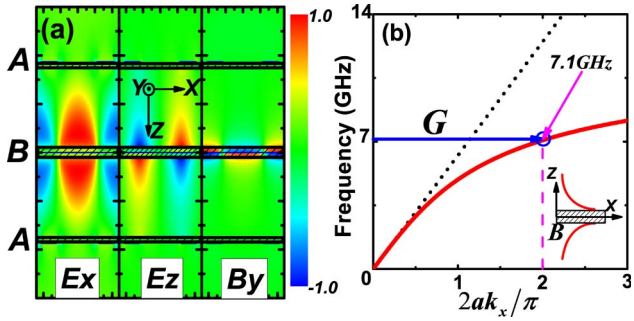

Fig. 3. (Color online) (a) Field distributions inside the structure (with $d = 8$ mm) calculated at 7.08 GHz. (b) Dispersion relation of the SPP on the B layer. The arrow represents a reciprocal vector provided by layer A.

calculations, consistent with an early theoretical analysis on a slightly different structure [20].

Understanding the physical mechanisms helps us manipulate these transmission peaks *freely* and *independently*. The two EMT peaks are dictated by the microstructure of layer A but are insensitive to the periodicity, while the EOT peak is essentially determined by the periodicity of layer A. Simultaneously, three peaks also exist for the polarization $\vec{E} \| \hat{y}$, but at different frequencies. Therefore, we purposely adjusted the structure to make the EOT peak for x-polarization coincident with the second EMT peak for y-polarization. Specifically, the EMT peaks may blueshift (redshift) if the parameter g is decreased (increased), while the EOT peak may blueshift (redshift) if the parameter a is decreased (increased). The transmission spectra (including amplitudes and phases) through the optimized system are shown in Fig. 4 as solid lines for two incident polarizations. We note that the system is *perfectly transparent* for both polarizations at ~5.1 GHz. However, the transmission phase changes are $\varphi_x \sim 0°$ and $\varphi_y \sim 90°$ for the two polarizations. The physics underlying such a big difference is that the transparencies are dictated by different principles. For x-polarization the transparency is the EOT type, and thus φ_x is nearly 0, since the role of layer A is to provide a reciprocal vector and it does not need to have a large permittivity. In contrast, the transparency for y-polarization is the EMT type [see Fig. 4(b)], so φ_y must be large, since a large permittivity is required for layer A to compensate

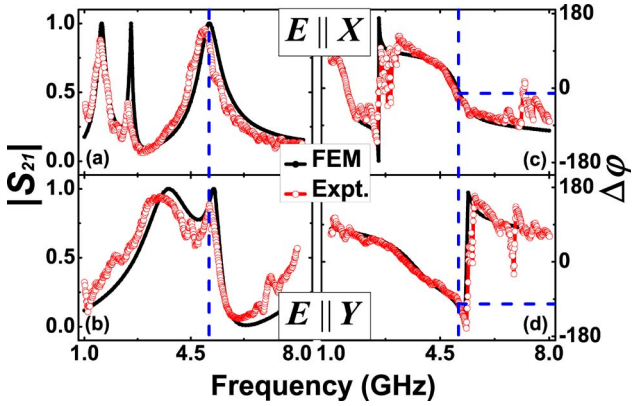

Fig. 4. (Color online) For the optimized structure (same values as in Fig. 1, with $d = 0$ mm), simulated (solid curves) and measured (circles) spectra of transmission amplitudes and phases for two incident polarizations.

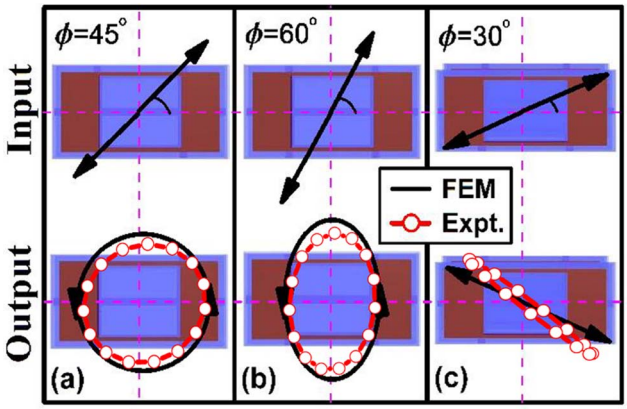

Fig. 5. (Color online) Simulation (solid curves) and experimental (circles) results for three typical polarization manipulation effects: (a) linear-to-circular conversion, (b) linear-to-elliptical conversion, and (c) polarization direction rotation.

the negative permittivity of layer B, based on the EMT [13]. Such a big $\Delta\varphi$ is remarkable considering our system is only $\lambda/20$ thick. In contrast, ordinary polarization-modulation materials are much thicker than wavelength to achieve this phase difference [3]. Although previously designed thin metamaterials [8–12] can also realize such a big phase difference, those systems do not support *perfect* transmissions, and the physical mechanisms are quite different.

Microwave experiments were performed to verify the theoretical predictions. We fabricated metamaterial samples in sizes 48 cm × 48 cm based on the designs [see pictures for layers A and B shown in Figs. 1(b) and 1(c)] and measured the transmission spectra of the ABA structure using a vector network analyzer (Agilent E8362C PNA). The measured $|S_{21}|$ and $\Delta\varphi$ are plotted as open circles in Fig. 4 for two incident polarizations. Excellent agreement is found between experimental and simulation results. In particular, experiments confirmed that the transmittance is maximized for both polarizations around 5.1 GHz, but with a phase difference of ~90°. However, the maximum transmissions cannot reach 100% as predicted by the theory, probably due to the imperfections in the sample and the loss of the substrate.

The designed system can realize many fascinating polarization manipulation effects. As shown by both simulations and experiments in Figs. 5(a) and 5(b), an input linearly polarized wave (LPW) with $\phi = 45°$ ($\phi = 60°$) becomes a circularly (elliptically) polarized wave after passing through our system. Put two ABA systems together, and the whole system can achieve a doubled phase difference (~180°) for two incident polarizations. Therefore, an LPW keeps its linear polarization, but with the polarization direction rotated after passing through the system. An example is shown in Fig. 5(c), where the **E** direction is rotated from $\phi = 30°$ to $\phi = 150°$ after passing through the device. Such a rotation angle is remarkable, since the thickness of our device is only $\lambda/10$ [3].

In short, we demonstrated both experimentally and theoretically that an ultrathin metamaterial could manipulate EM wave polarizations efficiently in transmission geometry.

W.-J. Sun and Q. He equally contributed to this work. This work was supported by the National Natural Science Foundation of China (NSFC) (Nos. 60725417, 60990321) and Shanghai Science and Technology Committee (08dj1400302).

References and Notes

1. M. Born and E. Wolf, *Principles of Optics* (Cambridge University Press, 1999).
2. B. Z. Katsenelenbaum, *High-Frequency Electrodynamics* (Wiley-VCH, 2006).
3. R. Guenther, *Modern Optics* (Wiley, 1990).
4. J. B. Pendry, A. J. Holden, W. J. Stewart, and I. Youngs, Phys. Rev. Lett. **76**, 4773 (1996).
5. J. B. Pendry, A. J. Holden, D. J. Robbins, and W. J. Stewart, IEEE Trans. Microwave Theory Tech. **47**, 2075 (1999).
6. D. R. Smith, W. J. Padilla, D. C. Vier, S. C. Nemat-Nasser, and S. Schultz, Phys. Rev. Lett. **84**, 4184 (2000).
7. J. Hao, Y. Yuan, L. Ran, T. Jiang, J. A. Kong, C. T. Chan, and L. Zhou, Phys. Rev. Lett. **99**, 063908 (2007).
8. M. Beruete, M. Navarro-Cía, M. Sorolla, and I. Campillo, J. Appl. Phys. **103**, 053102 (2008).
9. T. Q. Li, H. Liu, T. Li, S. M. Wang, F. M. Wang, R. X. Wu, P. Chen, S. N. Zhu, and X. Zhang, Appl. Phys. Lett. **92**, 131111 (2008).
10. T. Li, H. Liu, S. M. Wang, X. G. Yin, F. M. Wang, S. N. Zhu, and X. Zhang, Appl. Phys. Lett. **93**, 021110 (2008).
11. J. Y. Chin, M. Z. Lu, and T. J. Cui, Appl. Phys. Lett. **93**, 251903 (2008).
12. Y. Ye and S. He, Appl. Phys. Lett. **96**, 203501 (2010).
13. L. Zhou, W. Wen, C. T. Chan, and P. Sheng, Phys. Rev. Lett. **94**, 243905 (2005).
14. COMSOL Multiphysics 3.5, developed by COMSOL (network license 2008).
15. T. W. Ebbesen, H. J. Lezec, H. F. Ghaemi, T. Thio, and P. A. Wolff, Nature **391**, 667 (1998).
16. I. R. Hooper and J. R. Sambles, Phys. Rev. B **70**, 045421 (2004).
17. C. A. M. Butler, J. Parsons, J. R. Sambles, A. P. Hibbins, and P. A. Hobson, Appl. Phys. Lett. **95**, 174101 (2009).
18. S. A. Maier, *Plasmonics: Fundamentals and Applications* (Springer, 2007).
19. Two SPP branches exist on the B layer, exhibiting odd and even symmetries. Here we only plot the even-mode SPP dispersion, since the other branch is at a higher frequency range.
20. A. M. Dykhne, A. K. Sarychev, and V. M. Shalaev, Phys. Rev. B **67**, 195402 (2003).